Model Ziegler−Natta Polymerization Catalysts Fabricated by Reactions of Mg Metal and $TiCl_4$: Film Structure, Composition, and Deposition Kinetics

Seong Han Kim and Gabor A. Somorjai*

Department of Chemistry, University of California at Berkeley, and Materials Science Division, Lawrence Berkeley National Laboratory, Berkeley, California 94720

Received: December 20, 1999; In Final Form: February 29, 2000

The film structure, composition, and deposition kinetics of model Ziegler−Natta polymerization catalysts produced by chemical vapor deposition have been studied using temperature-programmed desorption (TPD), Auger electron spectroscopy (AES), and X-ray photoelectron spectroscopy (XPS). Redox reactions of metallic Mg and $TiCl_4$ deposited from the vapor phase on a Au substrate produce the model catalysts composed of titanium chloride and magnesium chloride ($TiCl_x/MgCl_2$). The low solubility of $TiCl_x$ in $MgCl_2$ leads to the formation of a $TiCl_x$ monolayer on top of $MgCl_2$ multilayers characteristic of the supported catalysts. The $TiCl_4$/Mg flux ratio during the deposition controls the oxidation state distribution and surface coverage of $TiCl_x$ species of the deposited film. The conversion of Mg to $MgCl_2$ is completed in the codeposition process while it is incomplete in the sequential deposition process due to a kinetic barrier for chlorine diffusion. Upon heating the sequentially deposited film, the surface $TiCl_x$ (Ti^{4+}) species react with metallic Mg atoms in underlayers to complete the redox reaction. In the case of the codeposited film, the surface $TiCl_x$ species desorb as $TiCl_4$ at temperatures higher than 430 K. After exposure to triethylaluminum ($AlEt_3$) cocatalyst, the model catalyst films are active for propylene polymerization.

I. Introduction

The titanium-based Ziegler−Natta catalytic system is extensively used in industry for polyethylene and polypropylene production. A high-surface-area industrial catalyst consists of $TiCl_4$ supported on activated $MgCl_2$ particles.[1] $MgCl_2$ is considered an efficient dispersant of active titanium, and its electronic interaction with the active titanium species is believed to enhance polymerization activity.[2,3] Identification and characterization of polymerization sites on supported catalysts have long been attempted mostly in indirect ways such as polymer product analyses.[1] However, considering the heterogeneous nature of catalysis, knowledge of catalyst surface properties, unobtainable from product analyses, is of paramount importance in the unambiguous description of active sites and understanding of polymerization mechanisms.[4,5] Unfortunately, surface-sensitive techniques employing electrons or ions cannot be employed directly for surface characterization of the high-surface-area supported catalysts, composed of small particles of insulating materials, due to charging problems. Thus, preparation of a model system on an electrically conducting and chemically inert surface is necessary for surface science studies of the active sites of the Ziegler−Natta polymerization catalysts.[6−8] We prepare a monolayer (ML) film of titanium chloride on top of a $MgCl_2$ film deposited on a gold foil in order to reproduce the structure of the supported catalysts.

As a model substrate, a $MgCl_2$ thin film deposited by thermal evaporation has been studied under ultra-high-vacuum (UHV) conditions. The $MgCl_2$ multilayer film has a surface structure of the α-$MgCl_2(001)$ basal plane that is chlorine terminated.[9−11] $TiCl_4$ does not chemisorb on this Cl-terminated film in UHV.[12] A 1000 eV electron irradiation on $MgCl_2$ has been shown to be an effective way to grow a titanium chloride film stable in the polymerization temperature range (300−350 K).[13,14] However, electron irradiation of the $MgCl_2$ film during the $TiCl_4$ exposure allows growth of titanium chloride multilayers thick enough to completely attenuate the Mg signal in X-ray photoelectron spectroscopy (XPS).[14] This film structure is rather closer to a $TiCl_3$-based catalyst that is not as active as the $MgCl_2$-supported catalyst.[1]

Without using high-energy electrons, titanium chloride films have been reported to grow on the $MgCl_2$ film by codeposition of metallic Mg atoms during $TiCl_4$ exposure.[15] In this case, Mg^{2+} ions were detected in XPS, implying that the model system is much closer to the $MgCl_2$-supported-catalyst system. The titanium chloride film on $MgCl_2$ can also be formed in UHV by exposure of metallic Mg film to $TiCl_4$. The simplicity of these synthetic methods and the closeness of the model catalyst composition to the supported catalyst provided us with the incentive to employ the reaction of Mg metal and $TiCl_4$ for synthesis of model catalysts with various Ti oxidation state distributions.

In this paper, we present detailed studies of chemical vapor deposition of model Ziegler−Natta polymerization catalysts using Mg metal and $TiCl_4$. Temperature-programmed desorption (TPD), Auger electron spectroscopy (AES), and XPS have been used to study their structure, composition, and deposition kinetics. The model catalysts produced in this way are active for propylene polymerization after exposure to triethylaluminum ($AlEt_3$) cocatalyst. TPD and AES results reveal that the UHV-prepared model catalyst film has titanium chloride on top of magnesium chloride characteristic of the structure of high-surface-area $MgCl_2$-supported catalysts. Upon heating the model catalysts, the surface titanium chloride species undergoes two competing reactions, desorption and reduction, depending on the film composition. The titanium oxidation state distribution, measured with XPS, can be controlled by changing the $TiCl_4$/Mg flux ratio during deposition and postdeposition annealing.

10.1021/jp994441k CCC: $19.00
Published on Web 05/19/2000

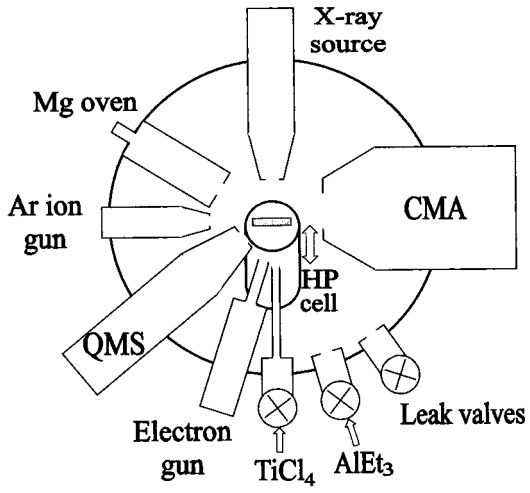

Figure 1. Schematic diagram of the experimental apparatus.

II. Experimental Section

A schematic diagram of the experimental apparatus is shown in Figure 1. The UHV chamber was pumped by a 2000 L/s diffusion pump and maintained a base pressure of about 1×10^{-9} Torr. This UHV chamber was equipped with a sputter ion gun for surface cleaning, an X-ray source and a double-pass cylindrical mirror analyzer (CMA) with a coaxial electron gun for XPS and Auger electron spectroscopy (AES), a quadrupole mass spectrometer (QMS) for residual gas analysis and TPD. A commercially available sample manipulator provided three-dimensional translation and 360° rotation of the sample. The chamber also had three leak valves for gas exposure, a Knudsen cell for Mg dosing, an electron flood gun for electron beam irradiation onto the sample, and an internal high-pressure reaction cell (HP) for in situ polymerization.

A polycrystalline Au foil (1.2 cm^2) was spot welded onto Au wires which were spot welded onto Ta posts that were attached to liquid N_2 cooled electrodes. This assembly made it possible to heat the Au foil resistively to 1000 K and to cool to 100 K within less than 1 min. A K-type thermocouple was attached to the back of the foil for temperature measurement. The Au foil was cleaned with Ar ion sputtering followed by annealing at 900 K. Surface cleanliness was checked with XPS and AES.

$TiCl_4$ and *n*-hexane were purified by several freeze−pump−thaw cycles. A triethylaluminum ($AlEt_3$) source was purified by mechanical pumping while being cooled with an ice−water bath. Polymer-grade propylene was purified by flowing through an oxygen/water trap before use.

Gas admittance into the UHV chamber was controlled with leak valves facing the sample. The leak valve used for $TiCl_4$ exposure was equipped with a 1/8-in. stainless steel tube that extended to the front of the sample to minimize chamber contamination. The TPD analysis of *n*-hexane uptake behavior determined the pressure enhancement of the $TiCl_4$ doser to be a factor of ~3 compared to the others. Nominal pressures of $TiCl_4$ reported in this paper, $P(TiCl_4)$, were readouts of the nude ion gauge, located about 20 cm away from the sample, without correction for ionization sensitivity and dosing geometry.

Mg was evaporated from the Knudsen cell composed of a resistively heated graphite crucible. Adjusting the crucible temperature (T_{Mg}) and exposure time controlled the Mg dose. The Mg flux was estimated from the attenuation of the 239 eV Au AES peak.[16] With a crucible temperature of 600 K and at an incidence angle of 60° with respect to the surface normal, the 10 min deposition of Mg reduced the Au AES intensity by 75%. Assuming the thickness of 1 ML of Mg as 2.6 Å, half the *c* parameter of the hexagonal close packed unit cell of Mg, and the inelastic mean free path of the 239 eV electron in the Mg crystal to be 8.2 Å,[17] the 75% attenuation corresponds to about 3 ML of Mg on top of Au. Assuming a unity sticking probability of Mg and considering the number density of Mg in the close-packed surface to be 1.1×10^{15} atoms/cm^2, the Mg atom flux on the surface is calculated to be about 6×10^{12} atoms/cm^2 s at the above condition.

The model catalysts composed of titanium chloride and magnesium chloride, $TiCl_x/MgCl_2$, were prepared by chemical vapor deposition of $TiCl_4$ and Mg on the Au foil at 300 K. Two deposition sequences were employed: (1) codeposition and (2) sequential deposition. For the codeposition of $TiCl_x/MgCl_2$, the substrate was rotated to face both the Mg Knudsen cell and the $TiCl_4$ doser at 60° with respect to the surface normal. Mg was evaporated from the Knudsen cell during the $TiCl_4$ exposure. In the case of sequential deposition, Mg was first deposited onto the Au surface at 60° with respect to the surface normal, and then the Mg deposit was exposed to $TiCl_4$.

In TPD experiments, the deposited film was resistively heated at a ramp rate of 4 K/s. The QMS ionizer was covered with a shroud that had an aperture of about 5 mm, positioned about 1 cm from the surface, to discriminate background desorption. QMS signals, up to 5 masses, were recorded with a computer. In XPS analysis, the Al Kα radiation (1486.6 eV) was used and the angle between the surface normal and the CMA axis was 35°. The Au $4f_{7/2}$ peak at 84 eV was taken as a reference for the energy scale. The XPS spectra of Ti reported in the following section have been background subtracted and deconvoluted into a series of synthetic peaks (67% Gaussian and 33% Lorentzian; fwhm = 2.3 eV) that represent the photoelectron emission from different oxidation states.[18] The fitting parameters for the synthetic peaks were obtained from the Ti 2p spectrum of $TiCl_4$ physisorbed at 100 K. In AES analysis, the primary electron beam irradiated the surface only during the scan and its current was kept lower than 1 μA.

As a reference substrate for TPD and XPS, $MgCl_2$ multilayers were deposited on Au at 300 K by thermal evaporation of $MgCl_2$ from a separate Knudsen cell, until no Au signal was observable in AES. XPS confirmed the stoichiometry of the $MgCl_2$ film.

Propylene polymerization was performed in the HP cell. First, the model catalyst was exposed to about 1 Torr of $AlEt_3$ at 300 K. After pumping out $AlEt_3$, propylene (about 760 Torr) was introduced into the HP cell and the catalyst temperature was increased to 340 K. Polymerization was carried out with 800 Torr of propylene for 14 h. The polypropylene film produced on the model catalyst was analyzed with XPS and TPD in UHV or retrieved for Raman spectroscopy in air.

III. Results

III-1. Propylene Polymerization on Model Catalysts. The reaction of Mg with $TiCl_4$ produced model catalysts composed of titanium chloride and magnesium chloride ($TiCl_x/MgCl_2$) films on the inert substrate (Au foil). These catalysts were activated after contact with the $AlEt_3$ cocatalyst for 3 min.[19] Polymerization was carried out in the absence of cocatalyst in the gas phase. Figure 2 shows the XPS, TPD, and Raman spectrum of polypropylene films grown on the model catalysts prepared by codeposition of Mg and $TiCl_4$. XPS shows only the carbon peak of the polymer. The absence of the substrate (Au) and catalyst (Mg, Ti, and Cl) peaks indicates that the polymer film is thick.[20] When heated in UHV, the polypropylene

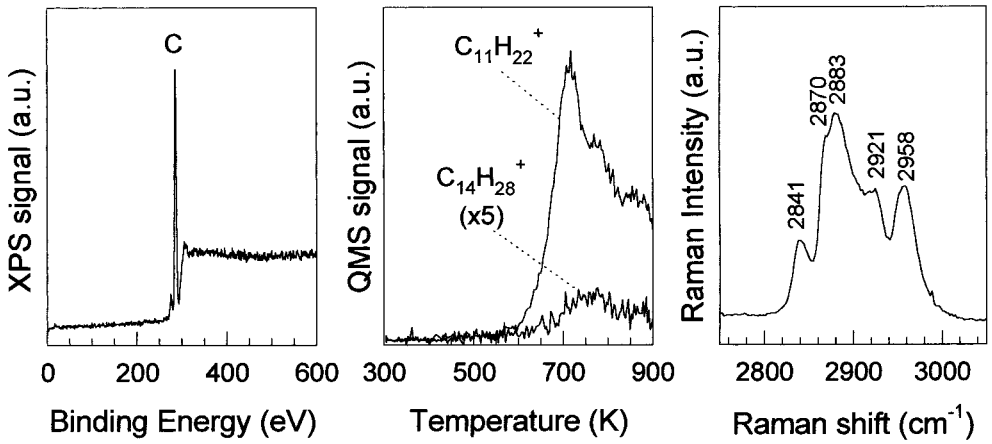

Figure 2. XPS, TPD, and Raman spectrum of the polypropylene film grown on the $TiCl_x/MgCl_2$ model catalyst activated by exposing to ~1 Torr of $AlEt_3$ for 3 min at 300 K. Polymerization was carried out with 800 Torr of C_3H_6 for 14 h at a catalyst temperature of 343 K.

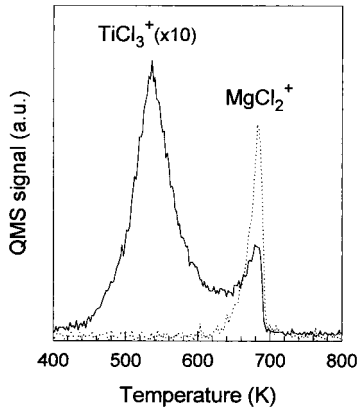

Figure 3. TPD profiles of $TiCl_3^+$ (153 amu) and $MgCl_2^+$ (94 amu) from $TiCl_x/MgCl_2$ prepared by codeposition at 300 K. Heating rate = 2 K/s. Deposition conditions: T_{Mg} = 600 K; $P(TiCl_4) = 2 \times 10^{-7}$ Torr; time = 5 min. To avoid data congestion, only $TiCl_3$+ is shown for $TiCl_x$+.

degrades at temperatures higher than 600 K and desorbs as small alkene fragments. Alkane desorption peaks are at least 1 order of magnitude smaller than corresponding alkene peaks (data not shown). There is no hydrocarbon desorption peak observable at the catalyst desorption temperature (see below), indicating that the thermal stability of the polypropylene film produced is governed not by the catalyst but by the polymer itself.[21] In the Raman spectrum of the polypropylene film produced on the model catalyst, the peaks at 2841, 2870−2883, 2921, and 2958 cm^{-1} can be assigned to $\nu_s(CH_2)$, $\nu_s(CH_3)$, $\nu_{as}(CH_2)$, and $\nu_{as}(CH_3)$, respectively, of the macromolecular chain.[22] No peak due to unsaturated end groups is observed.

In the following sections, the detailed TPD and XPS results of the $TiCl_x/MgCl_2$ model catalyst films prepared by two deposition methods will be described in light of film structure and composition. The surface structure and roughness of the film will be the subject of a future publication.[8−10,23−24]

III-2. TPD and XPS Characterization of the Codeposited Films. A typical TPD data of $TiCl_x/MgCl_2$ films prepared by codeposition is presented in Figure 3. The $MgCl_2$ desorption profile exhibits an exponential rise in the initial desorption rate accompanied by a sharp falling edge characteristic of multilayer desorption. Using zero-order kinetics, the desorption energy of $MgCl_2$ from $TiCl_x/MgCl_2$ is calculated to be 45 ± 3 kcal/mol. It should be noted that the sublimation of pure $MgCl_2$ multilayer film on Au (data not shown) yields an activation energy of 53.4 ± 0.6 kcal/mol which is in agreement with the reported values.[9,25] The difference of about 8 kcal/mol in the $MgCl_2$ desorption energy will be discussed in section IV-1.

The titanium chloride desorption exhibits a feature of two desorption peaks: a low-temperature peak at 430 K < T < 640 K and a high-temperature peak at T > 640 K. In the case of the low-temperature peak, the relative intensities of $TiCl_x^+$ (x = 1, 2, 3, and 4) ions recorded in the multiplex TPD were close to the fragmentation ratio of the gas-phase $TiCl_4$ molecule in QMS and their profiles show a symmetric shape with a peak at 540 K. In the case of the high-temperature peak, the relative $TiCl_x^+$ ion intensities do not follow the $TiCl_4$ fragmentation ratio (see section III-3) and their desorption profiles are almost identical to that of $MgCl_2$. The same desorption profile for $TiCl_x$(T > 640 K) and $MgCl_2$ strongly suggests that some titanium species are so strongly bound to $MgCl_2$, most likely incorporated into the $MgCl_2$ lattice, that their desorption accompanies the sublimation of the $MgCl_2$ layers.

The origin of the low-temperature $TiCl_4$ desorption is different from the high-temperature desorption at T > 640 K. First, the symmetric shape of the $TiCl_3^+$ desorption profile (peaked at 540 K) is consistent with first-order desorption kinetics of the adsorbate on the surface. Second, this low-temperature desorption takes place below the $MgCl_2$ sublimation temperature. If the 540 K peak is due to diffusion of a $TiCl_x$ species present in the $MgCl_2$ layers to the surface, the desorption rate of such a species will depend on the heating rate of TPD, showing a smaller peak (T < 640 K) at a faster heating rate.[26] However, when the heating rate was increased from 2 to 8 K/s (data not shown), there was no change in the relative intensity ratio of low (<640 K) vs high (>640 K) temperature peaks, implying that the low-temperature desorption peak is not due to a diffusion-limited desorption of bulk $TiCl_x$ species. Therefore, it can be concluded that $TiCl_4$ desorbing at T < 640 K originates from the $TiCl_x$ species chemisorbed on the film surface, not embedded in the film.

The AES and XPS measurements of the model catalysts supported the above conclusion. In AES, the $TiCl_x/MgCl_2$ film showed a Ti_{LMM}/Mg_{KLL} ratio of 1.8 ± 0.1 at 300 K. After a 640 K annealing, this ratio decreased to 1.4 ± 0.4. Upon annealing at 640 K, the Mg signal intensity increased and the Ti signal intensity decreased in XPS. These results indicated that the surface region of the as-deposited film is Ti-rich in composition, which decreases to some extent after the annealing due to $TiCl_4$ desorption (Figure 3).

It should be noted that an electron-stimulated desorption process causes reduction in the Cl peak intensity during the AES

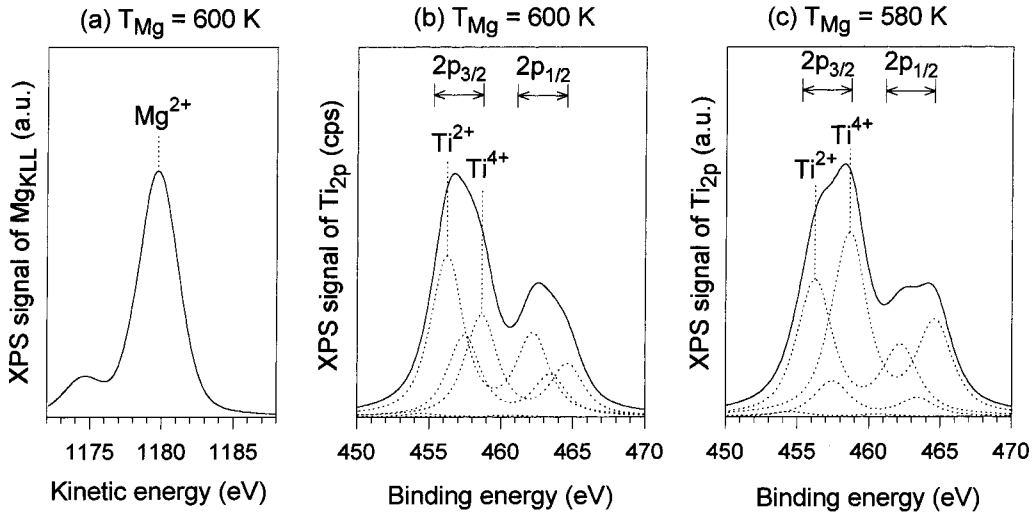

Figure 4. XPS spectra of the codeposited films: (a) the Mg_{KLL} peak and (b) the Ti_{2p} peak for the film deposited with T_{Mg} = 600 K and (c) the Ti_{2p} peak for the film deposited with T_{Mg} = 580 K. Other deposition conditions: $P(TiCl_4) = 1 \times 10^{-7}$ Torr; time = 10 min. The solid lines are the smoothed data after baseline correction. The dotted lines are deconvolution results (see text for details). The Ti oxidation states are marked only for 2+ and 4+ to avoid congestion.

TABLE 1: Ti Oxidation State Distribution (%) in the $TiCl_x/MgCl_2$ Film Deposited by Reaction of Mg with $TiCl_4$[a] (XPS Measurement: 300 K)

Mg oven temp (K)	deposition sequence	treatment	Ti oxidation state 4+	3+	2+	1+	0
580	codeposition	as-deposited	51	10	38	0	1
600	codeposition	as-deposited	29	24	46	0	1
600	codeposition	annealed[b]	8	12	65	6	9
580	sequencial	as-deposited	60	2	38	0	0
600	sequencial	as-deposited	31	6	60	3	0
600	sequencial	annealed[b]	0	6	80	14	0

[a] $P(TiCl_4) = 1 \times 10^{-7}$ Torr; deposition time = 10 min for each reactant. [b] Annealing temperature = 640 K.

measurement.[10,27] Due to this reason, the surface composition of chlorine could not be obtained from AES.

The oxidation states of Mg and Ti in the deposited film can be obtained from XPS. Figure 4a reports the Mg_{KLL} Auger peak in XPS for the catalysts prepared by codeposition at T_{Mg} = 600 K and $P(TiCl_4) = 1 \times 10^{-7}$ Torr for 10 min. Only one peak is observed at 1179.8 eV. The peak positions of Mg^{2+} and Mg^0 were determined as 1179.8 and 1185.5 eV from measurements of pure $MgCl_2$ and metallic Mg films. Therefore, the absence of the peak at 1185.5 eV indicates 100% conversion of the deposited Mg atoms to $MgCl_2$ (Mg^{2+}).

The titanium oxidation state distribution depends on the flux ratio of $TiCl_4$ to Mg during codeposition and postdeposition annealing. Figure 4b,c compares the Ti_{2p} XPS peaks of the codeposited films with different Mg flux (oven temperature) for a constant pressure of $TiCl_4$ (1×10^{-7} Torr). At a lower Mg oven temperature where the Mg flux is lower, the deposited film has more Ti^{4+} in the Ti oxidation state distribution. If the surface $TiCl_x$ species is removed by annealing at 640 K, the Ti oxidation states of the film reduce to mostly Ti^{2+}. The Ti oxidation state distributions, obtained by peak deconvolution, are summarized in Table 1.

III-3. $TiCl_x$ Deposition Kinetics in the Codeposition Process. The $TiCl_x$ deposition kinetics has been studied using TPD. Because the CMA averages the XPS signal over a wide range of takeoff angles in our experimental geometry, the film thickness information cannot be obtained from the XPS data. AES could not be used to measure the $TiCl_x/MgCl_2$ film thickness because the film is subject to the electron-stimulated desorption of chlorine.[10,27]

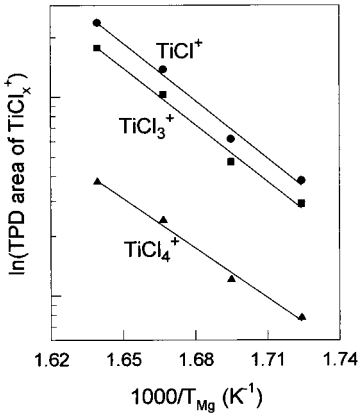

Figure 5. Uptake curve of $TiCl_x$ as a function of the Mg oven temperature during the codeposition process. Deposition conditions: T_{Mg} = 580, 590, 600, and 610 K; $P(TiCl_4) = 1 \times 10^{-7}$ Torr; time = 5 min.

The $TiCl_x$ amount detected in TPD increases linearly with the Mg flux during the codeposition process of $TiCl_x/MgCl_2$. Figure 5 reports the dependence of $TiCl_x$ deposition on the Mg oven temperature (T_{Mg}) at a constant $TiCl_4$ pressure (1×10^{-7} Torr, deposition time = 5 min). First, it should be noted that the Mg flux onto the Au substrate as a function of the Mg oven temperature follows the Clausius−Clapeyron equation.[28] In TPD of metallic Mg films on the Au substrate (data not shown), Mg desorbed in the temperature range from 450 to 550 K. Assuming a constant sticking probability for Mg deposition, the integrated peak area of the Mg TPD is proportional to the Mg flux onto the Au substrate during deposition. A plot of ln(Mg flux) vs $1/T_{Mg}$ yielded a slope of $\Delta H_{sub}/R$ from which the heat of Mg sublimation was calculated to be 31 ± 1 kcal/mol. This value is consistent with the reported value for Mg sublimation.[29,30] Therefore, the linearity in a plot of ln(deposited $TiCl_x$ amount) vs $1/T_{Mg}$ shown in Figure 5 can be interpreted as first-order kinetics of the $TiCl_x$ deposition to the Mg flux; i.e., the $TiCl_x$ deposition is proportional to the Mg flux onto the surface.

The uptake behavior of $TiCl_x$ as a function of the $TiCl_4$ pressure at a constant Mg flux ($\sim 6 \times 10^{12}$ atoms/cm^2 s at T_{Mg}

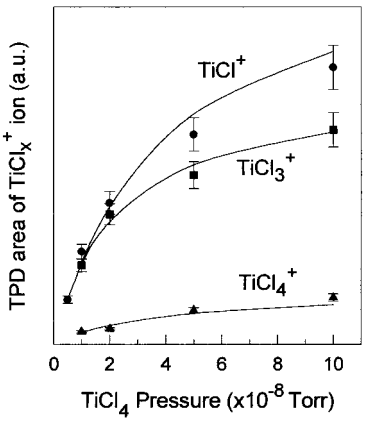

Figure 6. Uptake curve of $TiCl_x$ as a function of $TiCl_4$ pressure during the codeposition process. Deposition conditions: $P(TiCl_4) = 5 \times 10^{-9}$, 1×10^{-8}, 2×10^{-8}, 5×10^{-8}, and 1×10^{-7} Torr; $T_{Mg} = 600$ K; time = 5 min. The solid lines are drawn from fitting of the data to a Langmuir isotherm: $1/(\text{TPD area}) \propto 1/P(TiCl_4)$.

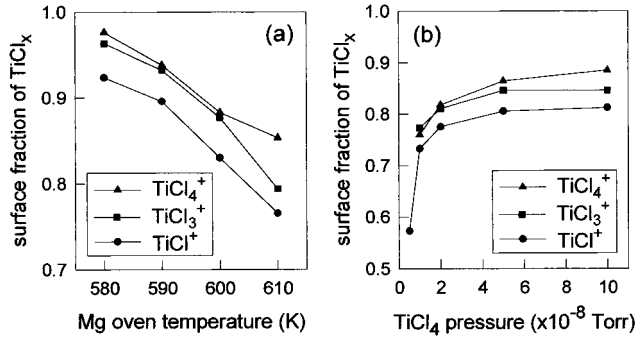

Figure 7. Surface fraction of $TiCl_x$ in the codeposited film as a function of (a) T_{Mg} and (b) $P(TiCl_4)$. Deposition conditions are listed in Figures 5 and 6.

= 600 K) is plotted in Figure 6. The deposition time was 5 min. The amount of $TiCl_x$ deposited in the film, proportional to the integrated TPD area, increases nonlinearly with $P(TiCl_4)$. The solid line in Figure 6 resulted from fitting of the TPD data to the Langmuir isotherm, i.e., $(\text{TPD area})^{-1} \propto P(TiCl_4)^{-1}$. The good agreement between the data and the fit implies that the $TiCl_4$ molecule impinging on the surface reacts and remains as $TiCl_x$ on the surface only if it finds a Mg (or MgCl intermediate) site where $TiCl_4$ can chemisorb.

Parts a and b of Figure 7 represent the surface fraction of $TiCl_x$ in the codeposited film as a function of Mg and $TiCl_4$ flux, respectively. The $TiCl_x$ surface fractions were obtained by dividing the integrated signal intensities below 640 K with the total intensities of the TPD profiles. At a constant $P(TiCl_4)$, the surface $TiCl_x$ fraction increases at lower Mg flux (lower T_{Mg}). For a given Mg flux ($\sim 6 \times 10^{12}$ atoms/cm^2 s), the surface fraction of $TiCl_x$ in the film increases with increasing the $TiCl_4$ pressure and levels off at $P(TiCl_4) > \sim 5 \times 10^{-7}$ Torr.

In Figure 7, it should be noted that the surface fraction value calculated for the $TiCl^+$ ion is always lower than that for $TiCl_3^+$, which is in turn lower than that for $TiCl_4^+$. The lower surface fraction values ($T < 640$ K) for the $TiCl_x^+$ ions containing less chlorine reflect desorption of chlorine-deficient species, $TiCl_y$ ($y \leq 3$), at $T > 640$ K, as well as $TiCl_4$. The $TiCl_y$ ($y \leq 3$) desorption is responsible for deviation of the relative intensities of $TiCl_x^+$ ions from the $TiCl_4$ fragmentation ratio at $T > 640$ K (as mentioned in Figure 3). The quantification of $TiCl_y$ ($y \leq 3$) species, relative to $TiCl_4$, was not possible because the

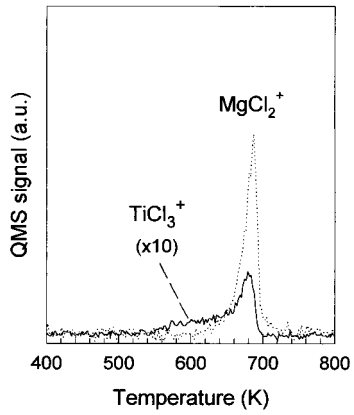

Figure 8. TPD profiles of $TiCl_3^+$ (153 amu) and $MgCl_2^+$ (94 amu) from $TiCl_x/MgCl_2$ prepared by sequential deposition at 300 K. Heating rate = 2 K/s. Deposition conditions: $T_{Mg} = 600$ K; $P(TiCl_4) = 2 \times 10^{-7}$ Torr; time = 5 min. To avoid data congestion, only $TiCl_3^+$ is shown for $TiCl_x^+$.

fragmentation ratios of $TiCl_y$ ($y \leq 3$) in the QMS are not available.

The amount of $TiCl_x$ incorporated in $MgCl_2$ layers has been estimated for the film codeposited with $T_{Mg} = 600$ K and $P(TiCl_4) = 1 \times 10^{-7}$ Torr for 10 min. Under this deposition condition, the amount of Mg atoms deposited on Au corresponds to 3 ML of Mg (see section II). From the crystallographic data, the Mg atom density is calculated to be 1.1×10^{15} atoms/cm^2 in 1 ML Mg and 8.7×10^{14} atoms/cm^2 in 1 ML of $MgCl_2$.[9,10] Therefore, complete conversion of Mg to $MgCl_2$ (see section III-2) will produce about 4 ML of $MgCl_2$. In Figure 7b, the $TiCl_x$ surface fraction is about 85% of the total $TiCl_x$ amount in the film. If we assume saturation coverage for the surface $TiCl_x$ species, the amount of $TiCl_x$ incorporated in $MgCl_2$ will be equal to about 0.17 ML. Therefore, assuming the number density of cations in 1 ML $TiCl_x$ to be the same as in 1 ML of $MgCl_2$, the $TiCl_x$ concentration in $MgCl_2$ is calculated to be about 4% ($Mg_{1-z}Ti_zCl_2$ with $z < 0.04$). It should be noted that this value is only an upper limit due to assumptions of saturation coverage for the surface $TiCl_x$ species and the titanium cation density in 1 ML $TiCl_x$. The stoichiometry of ionic crystals predicts lower cation densities for Ti^{3+} and Ti^{4+} in the unit cell than those of Ti^{2+} and Mg^{2+}. If the surface $TiCl_x$ species is mostly Ti^{4+}, the estimated upper limit for $TiCl_x$ incorporated in $MgCl_2$ will drop to about 2%.

III-4. TPD and XPS Characterization of the Sequentially Deposited Films. Figure 8 shows the TPD data of the sequentially deposited film. All deposition parameters were the same as in the codeposition process except the deposition sequence. Regardless of the deposition sequence, the $MgCl_2$ amount desorbing from the deposited film in TPD is the same in both cases. The heat of Mg sublimation is also the same for both films.

In contrast to $MgCl_2$, the $TiCl_x$ desorption profile in Figure 8 shows prominent differences from that of the codeposited film shown in Figure 3. The amount of the low-temperature desorption peak ($T < 640$ K) is significantly smaller than that of the high-temperature component ($T > 640$ K) in the sequentially deposited film, while it is much larger in the codeposited film. The behavior illustrated by the $TiCl_x$ TPD data clearly indicates that the deposition sequence has a profound effect on the thermal desorption of titanium chloride from the model catalyst.

Parts a and b of Figure 9 report the XPS spectra of Mg_{KLL} and Ti_{2p}, respectively, for the catalyst film prepared at 300 K

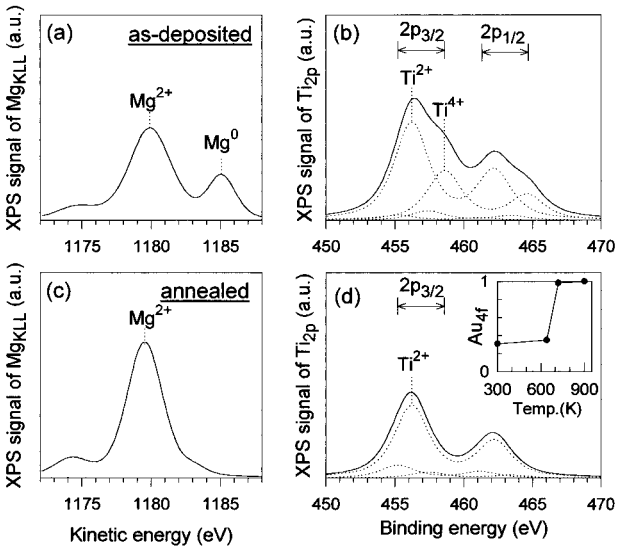

Figure 9. XPS spectra of the sequentially deposited film: (a) the Mg_{KLL} peak and (b) the Ti_{2p} peak for the as-deposited film (top) and (c) the Mg_{KLL} peak and (d) the Ti_{2p} peak of the film after annealing at 640 K (bottom). Deposition conditions: $T_{Mg} = 600$ K; $P(TiCl_4) = 1 \times 10^{-7}$ Torr; 10 min exposure for each reactant. The solid lines are the smoothed data after baseline correction. The dotted lines are deconvolution results (see text for details). The Ti oxidation states are marked only for 2+ and 4+ to avoid congestion. The inset to (d) shows the normalized intensity of Au_{4f} measured at 300 K as a function of annealing temperature.

by deposition of Mg with $T_{Mg} = 600$ K for 10 min followed by exposure to 1×10^{-7} Torr of $TiCl_4$ for 10 min. The as-deposited film contains some Mg^0, indicative of incomplete conversion of Mg to $MgCl_2$. However, the Ti oxidation state distribution of the sequentially deposited film is similar to that of the codeposited film within fitting errors (see Table 1). The titanium oxidation states measured in XPS are mostly 4+ and 2+. These results imply that the deposition sequence has only a marginal effect on the Ti oxidation state distribution.

After annealing the sequentially deposited film at 640 K, the Mg^0 peak disappears and the Mg^{2+} peak increases, which accompanies the reduction of the Ti oxidation states to mainly 2+ (Figure 9c,d). The inset to Figure 9d shows the Au_{4f} XPS signal intensity change as a function of annealing temperature. After annealing the film at 640 K, the substrate peak intensity increases very little, indicative of only minor mass loss from the film. This is consistent with the TPD result in Figure 8 that upon annealing to 640 K only a minor fraction of $TiCl_x$ is desorbed from the film. The substrate peak is completely recovered only after sublimation of $MgCl_2$ and $TiCl_x$ with a 720 K annealing.

Due to incomplete reaction between the deposited Mg and the gas-phase $TiCl_4$ molecules at 300 K, kinetic studies could not be performed for the sequential deposition process. However, the absence of the $TiCl_4$ desorption below 640 K in TPD (Figure 8) and the oxidation of unreacted Mg^0 and reduction in the Ti oxidation states upon annealing (Figure 9) provide insights to the sequential deposition kinetics at 300 K and thermal reactions during the anneal to 640 K, which will be discussed in section IV.

IV. Discussion

The chemical vapor deposition of Mg and $TiCl_4$ is a redox process where Mg is oxidized to Mg^{2+} forming $MgCl_2$ and Ti^{4+} in $TiCl_4$ is reduced to lower oxidation states with release of Cl^-. The results obtained in section III allow us to develop a detailed picture of the deposition and structure of $TiCl_x/MgCl_2$ film. In the following sections, the formation of the $Mg_zTi_{1-z}Cl_2$ ($z < 0.04$) support phase will be described first. Then the formation and reactions of the $TiCl_x$ catalyst phase will be discussed.

IV-1. $Mg_{1-z}Ti_zCl_2$ ($z < 0.04$) Support Phase. The redox reaction Mg and $TiCl_4$ is an exothermic and spontaneous reaction.[29,30] Since the co-deposition process completely converts of Mg to $MgCl_2$, the incomplete oxidation of Mg in the sequential deposition process (Figure 9a) indicates that there is a rate-limiting barrier for reaction of the deposited Mg with $TiCl_4$. The initial reaction takes place at the Mg film surface by adsorption of $TiCl_4$ on it and produces titanium chloride and magnesium chloride at the interface. These chloride layers are not active to abstract Cl^- from the $TiCl_4$ molecule.[11,31] Now the product layers separate the reactants and further reaction of the underlying Mg with $TiCl_4$ molecules can occur only via diffusion of surface Cl^- into underlayers. At room temperature, the diffusion of Cl^- through the product layer is not fast enough for complete oxidation of the Mg film during the $TiCl_4$ exposure. The $TiCl_x/MgCl_2$ layers act as a kinetic barrier for Cl^- diffusion at room temperature.

If the sequentially deposited film is annealed at 640 K, the interlayer diffusion of Mg and/or Cl^- is enhanced, leading to complete oxidation of unreacted Mg to $MgCl_2$ (Figures 8 and 9c). The diffusion of Mg from underlayers is quite obvious because the Mg adatoms on clean Au desorb at the temperature range of 450−550 K. The diffusion of Cl^- from the surface region into underlayers will also be accelerated at elevated temperatures.

In the codeposition process, however, the diffusional process does not play any significant role in deposition kinetics because Mg atoms are continuously provided to the reaction front from the gas phase. In other words, the reaction site for $TiCl_4$ is produced by Mg adsorption, rather than by Cl^- diffusion into $MgCl_2$ layers. Therefore, the kinetic barrier of chlorine diffusion is lifted and all Mg atoms adsorbed on the surface can be converted to $MgCl_2$ during the deposition.

After annealing at 640 K, the Ti species in the $Mg_{1-z}Ti_zCl_2$ ($z < 0.04$) phase has an oxidation state of mainly 2+ (Table 1). The incorporation of Ti^{2+} in $MgCl_2$, but not Ti^{3+} and Ti^{4+}, is in agreement with the solution energy of $TiCl_x$ in $MgCl_2$ calculated by Lin and Catlow.[31] The similar size and charge of Mg^{2+} and Ti^{2+} cations makes the substitution of Ti^{2+} for Mg^{2+} more favorable compared to Ti^{3+} and Ti^{4+}. Even for this annealed film, the AES ratio of Ti/Mg implies that the surface composition is still titanium rich. This could be attributed to the low solubility of $TiCl_2$ in $MgCl_2$. The solubility of $TiCl_2$ in the $MgCl_2$ solid is reported to be less than 0.5 wt % at 980 K.[32,33] The excess Ti^{2+} ions, incorporated into the $MgCl_2$ layer during codeposition at 300 K, appears to segregate to the film surface during annealing to 640 K.

The desorption energy of $MgCl_2$ from the $Mg_{1-z}Ti_zCl_2$ ($z < 0.04$) film is about 8 kcal/mol lower than that of the pure $MgCl_2$ multilayer film. This difference can be attributed to the presence of titanium chloride component in the $MgCl_2$ layers (Figure 3). The presence of a small amount of titanium ions (<4%) in the $MgCl_2$ layers is not surprising because the diffusion of Ti ions into the bulk $MgCl_2$ structure has already been reported by the conventional comilling process.[34] XPS data in Table 1 and Figure 9 shows that the titanium ions in the $MgCl_2$ layers are mainly Ti^{2+}. The Ti^{2+} substitution in the Mg^{2+} site weakens the bonding of the $MgCl_2$ layers,[35,36] lowering its sublimation

SCHEME 1

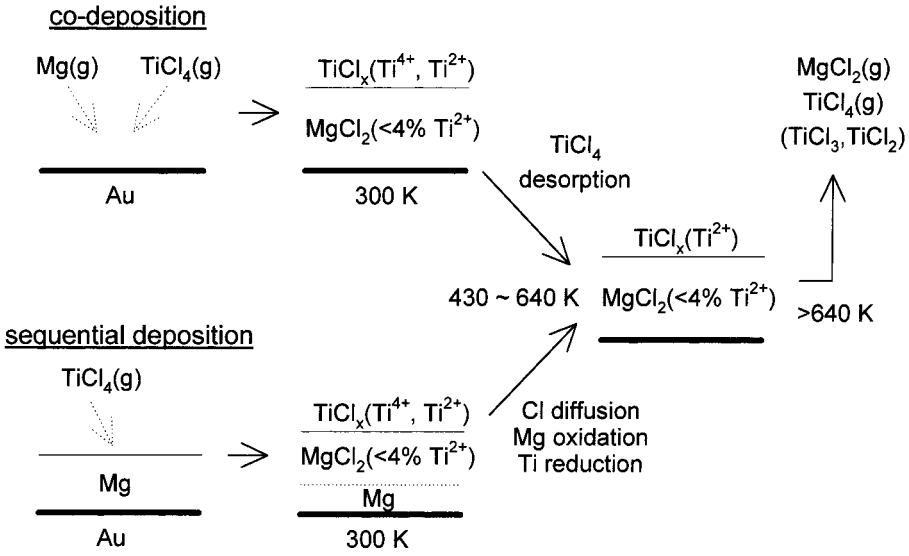

energy. During $MgCl_2$ sublimation at $T > 640$ K, the Ti^{2+} species desorb as chlorine-deficient molecules $TiCl_y$ ($y \leq 3$) as well as $TiCl_4$ (Figure 7). The $TiCl_y$ ($y \leq 3$) molecules are not as thermodynamically favored in the gas phase as $TiCl_4$. However, the stoichiometry of $MgCl_2$ layers with <4% Ti^{2+} does not have enough Cl to form $MgCl_2$(g) and $TiCl_4$(g).

IV-2. $TiCl_x$ Catalyst Phase on the Support. Despite the difference in preparation methods, the model catalysts produced by chemical vapor deposition in UHV reproduce the film structure of industrial catalysts produced by comilling $MgCl_2$ particles with $TiCl_4$.[1−3] The Ti-rich surface composition measured with AES and the first-order TPD profile of $TiCl_4$ below the $MgCl_2$ sublimation temperature (Figure 3) indicate that the $TiCl_x$ species are present at the surface of the deposited film, i.e., on top of the $Mg_{1-z}Ti_zCl_2$ ($z < 0.04$) layers. This can be rationalized by the low solubility of $TiCl_x$ in $MgCl_2$.[31,32] During deposition, the $TiCl_x$ phase segregates to the film surface that is composed of mostly $MgCl_2$.

Though the exact composition of the $TiCl_x/MgCl_2$ film cannot be obtained in the present experiment, overall composition seems not to follow the stoichiometry of the redox reactions such as $TiCl_4 + Mg \rightarrow TiCl_2 + MgCl_2$ or $2TiCl_4 + Mg \rightarrow 2TiCl_3 + MgCl_2$. Based on the film structure—a monolayer of $TiCl_x$ on multilayers of $MgCl_2$—and the Ti oxidation state distribution, the amount of $TiCl_x$ deposited in the film is much less than that of $MgCl_2$. This might be attributed to the exothermicity of redox reactions between Mg and $TiCl_4$. If some fraction of the heat of reaction is partitioned into the desorption channel of titanium chloride intermediates during deposition, this could lower the concentration of $TiCl_x$ in the deposited film. In fact, the desorption temperature of the surface $TiCl_x$ is about 150 K lower than the $MgCl_2$ layer.

The Ti oxidation state distribution in the as-deposited film can be controlled by changing the $TiCl_4$/Mg flux ratio during the deposition at 300 K. The higher the $TiCl_4$/Mg flux ratio, the more Ti^{4+} in the oxidation state distribution measured with XPS (Figure 4 and Table 1). This might be explained with the TPD result shown in Figure 7 that a lesser fraction of titanium is incorporated in $MgCl_2$ at lower Mg flux. After the 640 K anneal, only Ti^{2+} species are left in/on the model catalysts. The complete reduction of $TiCl_4$ to Ti, as in the Kroll process (metallothermic reduction at $T > 1000$ K),[37,38] does not occur under the present experimental conditions.

Upon heating, the fate of surface $TiCl_x$ species is different for two deposition sequences. Upon annealing to 640 K, the decrease of Ti^{4+} in the Ti oxidation state distribution is accompanied by $TiCl_4$ desorption in the case of the codeposited film (Figure 3 and Table 1), while it is accompanied by Mg oxidation, instead of $TiCl_4$ desorption, in the case of the sequentially deposited film (Figures 8 and 9). These results indicate that there are two competing reaction channels:

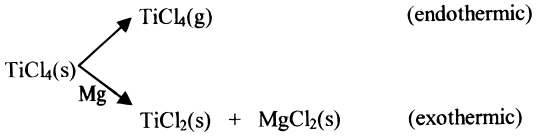

where (s) and (g) stand for surface and gas molecules, respectively. In the case of the codeposited film where no metallic Mg is available, the only possible reaction channel for the surface $TiCl_4$ species is desorption into vacuum as $TiCl_4$-(g). This channel is a kinetically irreversible process in UHV. However, in the case of the sequentially deposited film where unreacted Mg atoms are present in underlayers, the diffusion of Mg and/or Cl completes the thermodynamically favorable reaction, i.e., oxidation of Mg to $MgCl_2$ at the expense of Ti^{4+} reduction.

Scheme 1 illustrates the film structure and composition of the model Ziegler−Natta catalysts prepared by chemical vapor deposition of Mg and $TiCl_4$ on Au at 300 K and reactions in the catalysts upon heating.

V. Conclusions

Chemical reactions of Mg and $TiCl_4$ produce thin films of titanium chloride and magnesium chloride on the Au substrate. After exposure to triethylaluminum ($AlEt_3$) cocatalyst, these films are active for Ziegler−Natta polymerization. The titanium chloride TPD at different heating rates and relative ratio of Ti/Mg in AES indicate that the UHV-prepared model catalysts have the structure of high-surface-area catalysts, i.e., titanium chloride supported on magnesium chloride. The $TiCl_4$/Mg flux ratio during the deposition can be used to control the titanium oxidation state distribution. At higher $TiCl_4$/Mg ratio, more Ti^{4+} species is detected on the film surface. The amounts of $MgCl_2$ support phase and $TiCl_x$ catalyst phase depend on deposition

sequence as well as Mg and $TiCl_4$ exposures. In the sequential deposition process where $TiCl_4$ reacts with predeposited metallic Mg film, the $TiCl_x/MgCl_2$ layer at the interface acts as a kinetic barrier for Cl diffusion, leading to incomplete conversion of Mg to $MgCl_2$. Upon annealing, the $TiCl_x$ (Ti^{4+}) species at the film surface react, through interlayer diffusion, with metallic Mg atoms in underlayers. In the codeposition process, there is no such kinetic barrier because the reactants are supplied onto the product layers from the same side and the complete conversion of Mg to $MgCl_2$ is achieved during the deposition at 300 K. Upon heating of the codeposited film, the surface $TiCl_x$ species desorb as $TiCl_4$.

Acknowledgment. This work was supported by the Director, Office of Energy Research, Office of Basic Energy Sciences, Material Science Division, of the U.S. Department of Energy under Contract No. DE-AC03-76SF00098. The authors also acknowledge support from Montell USA, Inc.

References and Notes

(1) Dusseault, J. J. A.; Hsu, C. C. *J. Macromol. Sci.—Rev. Macromol. Chem. Phys.* **1993**, *C33*, 103, and references therein.
(2) Galli, P.; Barbe, P.; Guidetti, G.; Zannetti, R.; Marigo, A.; Bergozza, M.; Fichera, A. *Eur. Polym. J.* **1983**, *19*, 19.
(3) Gerbasi, R.; Marigo, A.; Martorana, A.; Zannetti, R.; Guidetti, G. P.; Baruzzi, G. *Eur. Polym. J.* **1984**, *20*, 967.
(4) Gassman, P. G.; Callstrom, M. R. *J. Am. Chem. Soc.* **1987**, *109*, 7875.
(5) Jenny, C.; Maddox, P. *Curr. Opin. Solid State Mater. Sci.* **1998**, *3*, 94.
(6) Gunter, P. L. J.; Niemantsverdriet, J. W.; Ribero, F. H.; Somorjai, G. A. *Catal. Rev.—Sci. Eng.* **1997**, *39*, 77.
(7) Goodman, D. W.; Rainer, D. R *J. Mol. Catal. A* **1998**, *131*, 259.
(8) Kim, S. H.; Somorjai, G. A. *Appl. Surf. Sci.*, in press.
(9) Fairbrother, D. H.; Roberts, J. G.; Rizzi, S.; Somorjai, G. A. *Langmuir* **1997**, *13*, 2090.
(10) Fairbrother, D. H.; Roberts, J. G.; Somorjai, G. A. *Surf. Sci.* **1998**, *399*, 109.
(11) Magni, E.; Somorjai, G. A. *Surf. Sci.* **1995**, *314*, L1078.
(12) Magni, E.; Somorjai, G. A. *Appl. Surf. Sci.* **1995**, *89*, 187.
(13) Magni, E.; Somorjai, G. A. *Surf. Sci.* **1996**, *345*, 1.
(14) Magni, E.; Somorjai, G. A. *J. Phys. Chem.* **1996**, *100*, 14786.
(15) Magni, E.; Somorjai, G. A. *J. Phys. Chem.* **1998**, *102*, 8788.
(16) Briggs, D.; Seah, M. P. *Practical Surface Analysis, Volume 1—Auger and X-ray Photoelectron Spectroscopy*, 2nd ed.; J. Wiley & Sons: Chichester, UK, 1990.
(17) Tanuma, S.; Powell, C. J.; Penn, D. R. *Surf. Interface Anal.* **1991**, *17*, 911.
(18) Mousty-Desbuquoit, C.; Riga, J.; Verbist, J. J. *Inorg. Chem.* **1987**, *26*, 1212.
(19) Magni, E.; Somorjai, G. A. *Surf. Sci.* **1997**, *377*, 824.
(20) In AFM measurements, the thickness of polypropylene films produced on our model catalysts was typically 1−4 μm with a root-mean-square roughness of about 100−300 nm (unpublished results).
(21) Novokshonova, L. A.; Kovaleva, N. Y.; Gavrilov, Y. A.; Krasheninnikov, V. G.; Leipunskii, I. O.; Zhigach, A. N.; Larichev, M. N.; Chebunin, M. V. *Polym. Bull.* **1997**, *39*, 59.
(22) Zhang, D.; Shen, Y. R.; Somorjai, G. A. *Chem. Phys. Lett.* **1997**, *281*, 394.
(23) Kim, S. H.; Tewell, C. R.; Somorjai, G. A. Submitted for publication in *Langmuir*.
(24) Kim, S. H.; Magni, E.; Somorjai, G. A. *Stud. Surf. Sci. Catal.*, in press.
(25) Pankratz, L. B. *Thermodynamic Properties of Halides*; US Department of Interior, Bureau of Mines: Washington DC, 1984.
(26) Kim, S. H.; Stair, P. C.; Weitz, E. *Langmuir* **1998**, *14*, 4156.
(27) Tokutaka, H.; Prutton, M.; Higginbotham, I. G.; Gallon, T. E. *Surf. Sci.* **1970**, *21*, 233.
(28) Chupka, W. A.; Inghram, M. G. *J. Phys. Chem.* **1955**, *59*, 100.
(29) Chase, M. W., Jr. *NIST-JANAF Themochemical Tables*, 4th ed.; *J. Phys. Chem. Ref. Data* **1998**, Monograph 9.
(30) Kubaschewski, O.; Alcock, C. B.; Spencer, P. J. *Materials Thermochemistry*, 6th ed.; Pergamon Press: Oxford, UK, 1993.
(31) Lin, J. S.; Catlow, C. R. A. *J. Mater. Chem.* **1993**, *3*, 1217.
(32) Smirnov, M. V.; Maksimov, V. S. *Elctrochem. Mol. Sol. Electrolytes* **1969**, *7*, 37.
(33) Komarek, K.; Herasymenko, P. *J. Electrochem. Soc.* **1958**, *105*, 214.
(34) Zakharov, V. A.; Makhtarulin, S. I.; Perkovets, D. V.; Moroz, E. M.; Mikenas, T. B.; Bukatov, G. D. *Stud. Surf. Sci. Catal.* **1986**, *25*, 71.
(35) Kashiwa, N. *Polym. J.* **1980**, *12*, 603.
(36) Kashiwa, N.; Toyota, A. *Polym. Bull.* **1984**, *11*, 471.
(37) Deura, T. N.; Wakino, M.; Matsunag, T.; Suzuki, R. O.; Ono, K. *Metall. Mater. Trans. B* **1998**, *29*, 1167.
(38) Okabe, T. H.; Waseda, Y. *JOM—J. Min. Met. Mater. Soc.* **1997**, *49* (6), 28.